Simulating the rheology of dense colloidal suspensions using dissipative particle dynamics

E. S. Boek* and P. V. Coveney
Schlumberger Cambridge Research, High Cross, Madingley Road, Cambridge CB3 0EL, United Kingdom

H. N. W. Lekkerkerker
van 't Hoff Laboratory, University of Utrecht, Padualaan 8, 3584 CH Utrecht, The Netherlands

P. van der Schoot
Max Planck Institute for Colloids and Interfaces, Kantstrasse 55, D-14513 Teltow-Seehof, Germany
(Received 11 October 1996)

The rheological properties of colloidal suspensions of spheres, rods, and disks have been studied using a mesoscopic simulation technique, known as dissipative particle dynamics (DPD). In DPD, a suspension is modeled as a system of large colloidal particles in a liquid of interacting point particles. For the calculation of hydrodynamic interactions, this method is computationally more efficient than conventional techniques using a continuum model for the solvent. Applying a steady-shear rate to the particulate suspensions, we have measured the viscosity as a function of shear rate and volume fraction of the suspended particles. The viscosity of a 30 vol % suspension of spheres displays characteristic shear-thinning behavior as a function of increasing shear rate. The values for the high- and low-shear viscosity are in good agreement with experimental data. For higher particulate densities good results are obtained for the high-shear viscosity, although the viscosity at low-shear rates shows a dependence on the size of the suspended spheres that we attribute to finite size effects. Dilute suspensions of rods and disks show intrinsic viscosities which are in excellent agreement with theoretical predictions. For concentrated suspensions of both rods and disks, the viscosity increases with the third power of the volume fraction. We find the same scaling behavior as predicted by Doi and Edwards [M. Doi and S. F. Edwards, *The Theory of Polymer Dynamics* (Oxford University Press, New York, 1986)] for rod suspensions in the semidilute regime. The DPD simulation technique emerges as a useful tool for studying the rheology of particulate suspensions. [S1063-651X(97)08203-2]

PACS number(s): 82.70.Dd, 47.50.+d, 66.20.+d, 02.70.−c

I. INTRODUCTION

The rheological properties of concentrated colloidal dispersions are of fundamental and widespread interest, with many industrial applications, ranging from foodstuffs and chemicals to the upstream and downstream parts of the oil industry. Within oil exploration and production, most of the fluids which are used are colloidal in nature: drilling fluids, cement slurries, fracturing fluids, and reservoir injection fluids are all important cases in point. The performance properties of these fluids depend in large measure on their component particulates: the control of these fluid properties evidently depends on an understanding of colloid rheology.

As a model colloidal suspension, the monodisperse hard-sphere system has been extensively studied, experimentally, theoretically, and by computer simulations. High quality experiments have been performed on well-characterized model hard-sphere systems [1]; theoretical and simulation approaches, on the other hand, generally have to assume highly idealized systems, such as dilute suspensions at low-shear rates, as full treatment of hydrodynamics is very difficult. Practical applications, however, often deal with concentrated dispersions at high-shear rates. Moreover, many colloidal particulates are not spherical. Therefore there has been recent interest in the rheology of suspensions of particles with various shapes and sizes. Experimentally, the study of shape effects in suspensions is difficult, because it is hard to synthesize anisotropic colloidal particles with a monodisperse size distribution. Recent work shows that polydispersity has a significant effect on the hydrodynamics of particulate suspensions [2–4]. Furthermore, the static and dynamic behavior of suspensions is usually enriched by colloidal interactions between the suspended particles. It has been shown that both attractive and repulsive interactions have a significant effect on the rheology of suspensions of spherical particles [5]. Recent experiments suggest that suspensions of rods [6] are even more sensitive to colloidal attractions than suspensions of spheres.

For these reasons computer simulations offer a powerful alternative to study particulate suspensions, as an intermediate between theory and experiment. Model particles, like spheres, and prolate and oblate ellipsoids, are easily generated in a simulation. Particles can be created that do not suffer from polydispersity, or from attractive colloidal interactions. Prolate ellipsoids can be considered as a model approximation of inflexible, rodlike particles, such as attapulgite or sepiolite clay particles in drilling muds, or molecules forming liquid crystalline phases. Likewise, oblate ellipsoids are a model representation of disklike clay particles with a low aspect ratio, such as laponite (synthetic hectorite), which can form highly thixotropic gels.

Most simulation methods used to date are based on a continuum model for the solvent (discretized for numerical

*Electronic address: boek@cambridge.scr.slb.com

analysis), such as Brownian [7] and Stokesian dynamics [8]. To simulate suspensions at high-shear rates, these techniques are computationally very intensive: the calculation of hydrodynamic interactions increases cubically with the number of suspended particles [8]. Therefore the results to date have been restricted to relatively small systems. Instead, in this paper we advocate a particle-based simulation of the solvent: by modeling a suspension as a system of large colloidal particulates in a solvent of point particles, the calculation of interactions only causes a linear increase of the computing time with the number of colloidal particulates. There have also been some simulations of colloidal systems using lattice-Boltzmann methods [9–11]. We show here that another mesoscopic simulation technique, dissipative particle dynamics (DPD), can be successfully applied to study the rheology of dense supensions of spheres, rods, and disks. This particulate simulation technique was originally developed by Hoogerbrugge and Koelman [12]. The method appears to show much promise in the simulation of hydrodynamic behavior of systems too complicated to be tackled by traditional methods, especially in the field of microscale hydrodynamic phenomena, where Brownian effects play an important role [13]. This would make the scheme useful especially in the field of simulations of dispersed systems, such as colloidal suspensions and polymer solutions. Indeed, in two subsequent papers [14,15], the originators of the dissipative particle dynamics method set out to prove this point. In particular, they showed that the DPD technique produces realistic rheological behavior for sphere suspensions at high-shear rates [14]. Other successful applications of the DPD technique include simulations of polymer solutions [15,16], immiscible fluids [17], and single phase fluid flow through a simple model porous medium [12].

In this paper we further validate the DPD method by calculating rheological properties of colloidal suspensions in three dimensions, at different shear rates, and for different shapes and sizes of the colloidal particulates. The viscosity of suspensions of spheres is investigated as a function of shear rate. In particular, we calculate the low-shear viscosity, as Koelman and Hoogerbrugge [14] only reported results for high-shear rates. Furthermore, we calculate the viscosities of suspensions of rods and disks as a function of volume fractions increasing up to 35%, and compare these with theoretical and, where available, experimental results. The paper is organized as follows: In Sec. II we will give an outline of the DPD method; in Sec. III the rheology of spheres, rods, and disks are discussed; in Sec. IV the simulation results are presented and in Secs. V and VI we discuss the results and present our conclusions.

II. DISSIPATIVE PARTICLE DYNAMICS

The dissipative particle dynamics (DPD) simulation method was developed by Hoogerbrugge and Koelman [12] for studying complex fluids and hydrodynamic phenomena. By introducing a lattice-gas automaton (LGA) time-stepping procedure into a molecular dynamics (MD) scheme, they were able to construct a stochastic particle model for an isothermal fluid system. This model is at the same time much faster than MD and very flexible with respect to the addition of model features. We will only describe the basic model here; for more details we refer to [12]. The model consists of N particles, moving in a continuum domain of volume V. As in MD, the system is determined by the positions $\mathbf{r}_i$ and momenta $\mathbf{p}_i$ of each particle. As in a LGA, the system is updated in discrete time steps δt consisting of an instantaneous collision followed by a propagation substep of duration δt. In the collision phase the momenta are simultaneously updated according to the stochastic rule

$$\mathbf{p}_i(t+\delta t)=\mathbf{p}_i(t)+\sum_j \Omega_{ij}\hat{\mathbf{e}}_{ij}, \tag{1}$$

where $\hat{\mathbf{e}}_{ij}$ is the unit vector pointing from particle j to particle i, and the scalar variable Ω_{ij} specifies the momentum transferred from particle j to particle i. In the propagation phase the particle positions change according to a free propagation

$$\mathbf{r}_i(t+\delta t)=\mathbf{r}_i(t)+\frac{\mathbf{p}_i(t+\delta t)}{m_i}\delta t, \tag{2}$$

with m_i being the mass of particle i. For systems of particles with equal mass, as in our case, the change in momentum Ω_{ij} can be written as

$$\Omega_{ij}=W(|\mathbf{r}_i-\mathbf{r}_j|)\{\Pi_{ij}-\omega(\mathbf{p}_i-\mathbf{p}_j)\cdot\hat{\mathbf{e}}_{ij}\}. \tag{3}$$

$W(r)$ is a dimensionless, non-negative ''weight'' function which is zero for $r>r_c$, where r_c is the radius beyond which the interparticle interaction vanishes. The function $W(r)$ is normalized such that its volume integral is $V/N=n^{-1}$, where n is the average number density of the particles. We choose $W(r)=(3/\pi r_c^3 n)(1-r/r_c)$ if $r<r_c$ and zero otherwise.

At least for a single phase system, the dynamics described by these equations satisfies the requirements for a valid fluid-dynamical model: both mass and momentum are conserved, while the equations of motion are isotropic and Galilean invariant so the macroscopically averaged system obeys the Navier-Stokes equations [12,18,20]. The specific choice for Ω_{ij} in Eq. (3) leads to a well-defined asymptotically attained equilibrium state. The first, stochastic, term within the braces on the right-hand side of Eq. (3) causes the system to heat up, while the second, dissipative, term tends to relax any relative motion. In more detail, the stochastic term Π_{ij} $(=\Pi_{ji})$ is a random number sampled from a distribution with mean $\langle\Pi_{ij}\rangle=\Pi_0$ and variance $\langle(\Pi_{ij}-\Pi_0)^2\rangle$. Thus $\Pi_{ij}=\Pi_0+\delta\Pi_{ij}$, where Π_0 represents a repulsive interaction, ensuring that the particles remain distributed homogeneously, while $\delta\Pi_{ij}$ causes fluctuations and prevents ordering of the system, that is it represents an effective Brownian motion. The dissipative term, containing the dimensionless number ω, causes friction and gives rise to a macroscopic viscosity. Both terms acting together have the effect of a thermostat: if the system gets too hot, the dissipative term (proportional to the relative motion of the particles) will dominate and cool the system, whereas if it becomes too cold, the Brownian term will dominate and drive the system to higher temperatures.

It has been shown that the property of detailed balance is satisfied by DPD, for the one-component case [18] and the multicomponent case [19], and therefore a Gibbsian equilib-

rium state is guaranteed to exist. We have verified the single particle velocity distribution for a three-dimensional DPD fluid with an average density of $nr_c^3=3$. Indeed, the velocity distribution matched the Maxwell-Boltzmann distribution perfectly. In a fluid of identical particles, one would expect a Maxwell distribution on very general grounds, characterized by the mean square velocity used to compute the temperature. However, Español and Warren [20] found that, using the original DPD model of Hoogerbrugge and Koelman, equipartition is not obeyed in a mixture of particles of different masses. They suggested two modifications to the basic DPD model to ensure that the DPD equilibrium state is the canonical ensemble. The first is reducing the length of the time step by a factor of 10, the second is the insertion of an extra factor of $2(1-r/r_c)$ in the dissipative term in the change in momentum [Eq. (3)], in order to satisfy the fluctuation-dissipation theorem. However, for hydrodynamic simulations it is not strictly necessary to be in the regime where Boltzmann statistics holds. In a sense this is the analog of the situation which pertains for virtually all multicomponent lattice-gas and lattice-Boltzmann automaton models, which do not satisfy detailed balance yet which describe hydrodynamic behavior well. We have checked this assumption by performing a few calculations with and without the suggested modifications to the algorithm: indeed it appears that the value of the viscosity of suspensions under shear (as described later) is not significantly affected. Therefore we have conducted our simulations using the original algorithm as described above.

Ω_{ij}, as defined in Eq. (3), can be regarded as an interparticle interaction term. The DPD interactions are very ''soft'' as compared with MD interparticle forces, which are characterized by steep short-range potential functions; the DPD particles are in fact to some extent ''transparent'' as there is no absolute volume exclusion. DPD is computationally advantageous relative to MD, because the soft DPD interactions allow particle motions of the order of a mean free path during each time step, whereas MD particle motions are constrained to smaller distances to accommodate the steep potentials. The DPD time step is typically two to three orders of magnitude larger than the time step in a MD scheme. The fluid particles in DPD should not necessarily be seen as representations of molecules, but are more abstract ''carriers of momentum.'' These fluid ''packets'' have a mesoscopic nature; they are large with respect to the molecular level, but small in comparison with gradients of fluid dynamical quantities of interest. Note that DPD should be regarded as based on a—highly idealized—microscopic model, which produces correct mesoscopic and macroscopic behavior (like LGA). By contrast, MD delivers correct microscopic, mesoscopic, and macroscopic behavior, the last two in principle rather than in practice. We have used the dissipative particle dynamics algorithm, as implemented in the Rheoflex code [21] by Hoogerbrugge and Koelman. Within the flexible environment of this fluid model, large solid objects of arbitrary shapes, such as suspended particulates, can be modeled by a local ''freezing'' of the fluid particles. Therefore these solid objects do not have perfectly smooth surfaces. ''Freezing'' of the fluid particles is achieved in the following way: following a collision, the momenta of all ''frozen'' particles comprising a solid object are summed and redistributed over these particles, according to the Euler equations for rigid-body motion. In the subsequent propagation phase all these particles move together as a solid object, depending on the forces exerted by the surrounding fluid particles. In order to measure the viscosity of a suspension, a macroscopic steady-shear flow regime is imposed on the fluid. Steady uniform shear is simulated by using Lees-Edwards sliding periodic boundary conditions [22] and the stress tensor is then calculated at each time step: the virial expression for the stress tensor consists of contributions from the particle collisions and propagations, and from the solid objects. For a more detailed description of this rather complicated calculation, we refer to [14,21]. The shear viscosity of the suspension, ν, is related to the xy component of the stress tensor, σ_{xy}, in the following way:

$$\nu=-\sigma_{xy}/\dot{\gamma}, \tag{4}$$

where $\dot{\gamma}$ represents the imposed shear rate. The stress tensor is normalized by the number of particles, leading to a kinematic viscosity rather than a dynamic viscosity.

III. RHEOLOGICAL PROPERTIES OF DENSE PARTICULATE SUSPENSIONS

In this section we give an overview of theoretical expressions available for the viscosity of colloidal suspensions of various particulates, including spheres, prolate ellipsoids (rods), and oblate ellipsoids (disks).

A. Suspensions of spheres

The steady-state shear viscosity of a suspension of monodisperse spheres depends on two dimensionless groups [23]: the volume fraction $\phi=(4/3)\pi\rho a^3$ (where ρ is the number density [24] and a is the radius of the particles), and the Peclet number Pe, which is defined as

$$\mathrm{Pe}=\frac{\dot{\gamma}a^2}{D_0}=\frac{6\pi\eta_s a^3\dot{\gamma}}{k_BT}, \tag{5}$$

where D_0 is the Einstein diffusion coefficient, η_s is the solvent viscosity, and k_BT is the thermal energy. The Peclet number expresses the ratio between the hydrodynamic forces due to shear and the Brownian forces, which tend to restore the equilibrium configuration. In other words, the Peclet number expresses the ratio between two time scales: (1) the time needed to deform the dispersion structure by shear ($1/\dot{\gamma}$) and (2) the time scale of Brownian diffusion that restores the equilibrium configuration (a^2/D_0).

Therefore Pe measures the amount of departure from equilibrium. Except in a few limiting cases, the functional dependence of the viscosity on ϕ and Pe is not known theoretically.

One of the cases for which this dependence *is* known, is the viscosity of a dilute suspension of hard spheres. Einstein solved this problem in 1906 and 1911 [25] by calculating the extra energy dissipation in the fluid due to the presence of noninteracting spheres, and found

$$\eta_r=\eta/\eta_s=1+(5/2)\phi, \tag{6}$$

where η is the viscosity of the suspension and η_r is the reduced shear viscosity.

The effects of interactions between the suspended particles become significant at higher concentrations. This is where theoretical difficulties become severe. For the viscosity of less-than-dilute suspensions only approximate expressions have been derived, up to second order in an expansion of the viscosity in the volume fraction. This term includes contributions due to hydrodynamic interactions and Brownian motion and leads to [26,27]

$$\eta_r(\dot{\gamma}) = \eta/\eta_s = 1 + (5/2)\phi + k_2(\dot{\gamma})\phi^2. \tag{7}$$

The reduced viscosity η_r is now also a function of the applied shear rate, an effect which will become increasingly important with higher volume fractions ϕ. This dependence on the shear rate $\dot{\gamma}$ is included in the factor k_2, which has the following limiting behavior: (i) in the low-shear limit ($\dot{\gamma}\to 0$), where Brownian motion dominates, $k_2 = 6.2$ [27]; (ii) in the high-shear limit ($\dot{\gamma}\to\infty$), where the hydrodynamic contribution dominates, $k_2 = 5.2$ [26].

Equation (7), in which only pair interactions are included, is only valid at low concentrations; for higher concentrations, the hydrodynamics should be treated at the many-body level. This would involve calculation of ϕ^3 and higher order terms, which is theoretically cumbersome.

Many expressions have been proposed which relate the viscosity of concentrated suspensions in an empirical way to the volume fraction. The most famous is the Krieger-Dougherty relation [28] (which was later verified theoretically as well [29])

$$\eta_r = \left(1 - \frac{\phi}{\phi_{max}}\right)^{-[\eta]\phi_{max}}, \tag{8}$$

where ϕ_{max} is the maximum packing fraction or packing volume fraction (PVF), that is, the phase volume where the viscosity is infinite. Quemada [30] noted that experimentally the exponent $-[\eta]\phi_{max}$ is close to 2, which was confirmed by van der Werff and de Kruif [1].

Under such conditions, the use of numerical simulations may provide more insight into the complex behavior of dense suspensions. Barnes, Edwards, and Woodcock [31] have given an overview of the state of the art in simulations of dense colloidal suspension rheology. Using dissipative particle dynamics, Koelman and Hoogerbrugge [14] have simulated the shear flow of suspensions of solid spheres, up to volume fractions of 35%; recently this was extended to 45% [32]. They found viscosities that are in excellent agreement with the experimental data of van der Werff and de Kruif [1] for a sterically stabilized suspension of colloidal silica spheres. The authors only present simulation results for the viscosity at high Peclet numbers.

From an experimental point of view, the dimensionless Peclet number will always be very small for common laboratory shear rates, if small (a = 10 nm) colloidal particles are used [see Eq. (5)]. However, for larger particles, the Peclet number can be varied from small to large. This was exploited by van der Werff and de Kruif, who used silica spheres with radii varying from 28 to 110 nm. In the case of the smallest particles, the viscosity was measured in the range $10^{-4} < \mathrm{Pe} < 0.2$ and in that case only the low-shear viscosity was obtained. For the larger particles, measurements were done in the range $10^{-2} < \mathrm{Pe} < 10$ and a transition was observed from the low-shear viscosity $\eta(0)$ to the high-shear viscosity $\eta(\infty)$. The characteristic Peclet number Pe_c for this transition, defined as the value at which

$$\eta(\mathrm{Pe}_c) = \frac{1}{2}[\eta(0) + \eta(\infty)], \tag{9}$$

depends markedly on the volume fraction of the suspended spheres [1].

In the work described here, we have sought to further validate the DPD simulation technique by calculating the high-shear *and* low-shear viscosity of suspensions of spheres for volume fractions [33] $\phi = 0.3 - 0.4$, and determining Pe_c. The results for $\eta(0)$, $\eta(\infty)$, and $\eta(\mathrm{Pe}_c)$ will be compared with the experimental data of van der Werff and de Kruif [1]. Our results are presented in Sec. IV.

B. Suspensions of slender rods

The calculation of the viscosity of a suspension of rodlike particles is a long-standing problem. An important point is that the dependence of the viscosity on the solid volume fraction and the applied shear rate is stronger than for spherical particles. Shear thinning in suspensions of rods is mainly due to *orientational* ordering, whereas in sphere suspensions it is presumably due to *positional* ordering. In general, the hydrodynamic motions of nonspherical particles are described as ellipsoids of revolution, having their rotation axes properly oriented with respect to the flow direction. These ellipsoidal motions increase the amount of dissipated energy and therefore the viscosity of the fluid. The viscosity of a suspension of prolate ellipsoids of rotation, with semimajor axes $a \gg b = c$, can be written as an expansion up to first order in the volume fraction ϕ as follows:

$$\eta_R = \frac{\eta}{\eta_s} = 1 + [\eta]\phi, \tag{10}$$

with

$$\phi = \tfrac{4}{3}\pi a b^2 \rho, \tag{11}$$

where $\rho = N/V$ is the number density. Note that η_R is defined as the *reduced* viscosity, whereas $[\eta] = k_1$ is defined as the *intrinsic* viscosity. The intrinsic viscosity k_1 was evaluated by several authors. Taking Brownian motion into account, Onsager [34] obtained

$$k_1 = \frac{\frac{4}{15}\left(\frac{a}{b}\right)^2}{\ln\left(\frac{a}{b}\right)}. \tag{12}$$

Following Onsager, Simha [35] and Kuhn and Kuhn [36] independently calculated the viscosity from the energy dissipation of noninteracting rods. They found for the rod aspect ratio $f = a/b \gg 1$

$$k_1=\frac{f^2}{15[\ln(2f)-\frac{3}{2}]}+\frac{f^2}{5[\ln(2f)-\frac{1}{2}]}+c, \qquad (13)$$

with $c=\frac{14}{15}$ (Simha) and $c=1.6$ (Kuhn and Kuhn). Note that for $f\gg 1$, the Onsager result (12) is recovered from Eq. (13). The first term in Eq. (13) is the hydrodynamic contribution and the second term represents Brownian motion. Note that for $f\gg 1$, the Brownian contribution is exactly three times as large as the hydrodynamic contribution. In fact, for $f\gg 1$, the precise shape of the particles (ellipsoid, cylinder) is irrelevant; only the aspect ratio $f=\frac{a}{b}$ is important. This is a result of slender body theory [37].

A further step was taken by Berry and Russel [38], who managed to calculate the term of order ϕ^2 in the viscosity. This includes consideration of the effect of pairwise (hydrodynamic) interactions. They found (at low Peclet number):

$$\eta_R=\frac{\eta}{\eta_s}=1+k_1\phi+\frac{2}{5}k_1^2\phi^2, \qquad (14)$$

where the intrinsic viscosity $k_1=[\eta]$ is equal to the Onsager k_1 coefficient, as given in Eq. (12). The inclusion of the ϕ^2 term in Eq. (14) implies that this expression can be extended to somewhat higher concentrations than Eq. (10); nevertheless, it is still limited to the dilute regime. In a dilute solution of rods, the average distance between the rods, $\rho^{-1/3}$ (where ρ is the rod number density), is much larger than their length $2a$, i.e., $\rho\ll a^{-3}$.

At concentrations beyond the dilute regime, hydrodynamic interactions between many rods become important. When $\rho\gg a^{-3}$, the rods hinder each other in their rotational and translational motion: they become ''entangled.'' Stress relaxation is then believed to be dominated by how rapidly a rod can escape out of the ''cage'' formed by its neighbors. The cage concept was introduced by Doi and Edwards [39] for infinitely thin rods; the influence of finite rod widths has also been analyzed [40,41]. Within the cage model one finds the following expression for the viscosity of a congested solution of *cylindrical* rods:

$$\eta/\eta_s=\frac{32}{15\pi^2}\frac{f^6}{\beta\ln f}\phi^3(1-\alpha f\phi)^{-2}, \qquad (15)$$

in the limit $\rho\gg a^{-3}$, $f\gg 1$, and $\mathrm{Pe}\ll 1$, where α and β are to be taken as adjustable parameters [39–41]. The parameter β is equal to the square of the number of rods required to fully entangle a test rod orientationally. The parameter α measures, loosely speaking, how efficiently the ''free volume'' is reduced by the presence of the rods, and represents so-called ''log jamming'' effects. This expresses itself for instance in a reduced translational diffusion parallel to the rod direction, making it less easy for a rod to escape the cage. Comparison with real as well as computer experiments indicates that typically $\beta\cong O(10^3)$ [39,42,43] while $\alpha\cong O(10^{-1})$ [41,44]. Not too close to the isotropic-nematic phase transition, which roughly occurs at volume fractions $\phi\approx f^{-1}$ for hard rods [45], one can presumably neglect the term involving the parameter α, in which case Eq. (15) predicts that $\eta/\eta_s\propto\phi^3$. As we shall see in Sec. IV B, our simulations agree with this scaling behavior. We finally note that Eqs. (14) and (15) should, ideally, crossover smoothly.

In this paper, we have performed DPD simulations of suspensions of rods, to investigate how well these results agree with theoretical results for the dilute and concentrated regime [Eqs. (14) and (15)], as well as with available experimental data. Our results are presented in Sec. IV B.

C. Suspensions of disks

Just as rodlike particles can be modeled by prolate ellipsoids, disks can be described as oblate ellipsoids of revolution. In this way, the intrinsic viscosity $[\eta]$ of a dilute suspension of disks was evaluated by Kuhn and Kuhn [36]

$$[\eta]=\frac{4}{9}+\frac{32}{15\pi f}. \qquad (16)$$

For oblate ellipsoids, the aspect ratio $f=\frac{a}{b}<1$, a and b being the semimajor axes.

Güven [46] found a slightly different expression

$$[\eta]=\frac{5}{2}+\frac{32}{15\pi}\left(\frac{1}{f}-1\right)-0.628\left(\frac{1-f}{1-0.075f}\right). \qquad (17)$$

Rodlike particles with a high aspect ratio have a much larger intrinsic viscosity than disklike particles with high values of f^{-1}. For instance, for $f=100$ (f^{-1} for disks), the intrinsic viscosity would be roughly 600 for rods and 70 for disks, according to Eqs. (13) and (16). These values are much larger than $[\eta]=2.5$ for spherical particles. In Sec. IV C, we report on the results of our DPD simulations of disks.

IV. SIMULATION RESULTS

In order to simulate a suspension undergoing steady uniform shear, we have used sliding periodic boundary conditions with a three-dimensional simulation box, having a size of $30\times 30\times 30$ dimensionless units. We work in reduced units so that the time step δt, the interaction range r_c and the DPD particle mass m have a value of unity. We have used, as in [12], $\omega=4/3$, $\Pi_0=1/3$, and $\delta\Pi_{ij}$ was sampled from a homogeneous distribution on $[-1/3, 1/3]$. In all simulations, a particle density $n=3$ was used, corresponding to a total of 81 000 DPD particles.

A. Suspensions of spheres

In order to generate a suspension of solid spheres with a volume fraction of approximately 30%, 45 spheres with radius 3.5 were defined and randomly positioned within the simulation box. A snapshot of such a suspension undergoing shear is shown in Fig. 1. In view of the particle density $n=3$, each sphere contained about 540 ''frozen'' fluid particles. To investigate the possible effects of the (finite) size of the spheres, we also created suspensions containing 21 spheres of radius 4.5 and 68 spheres of radius 3.053, respec-

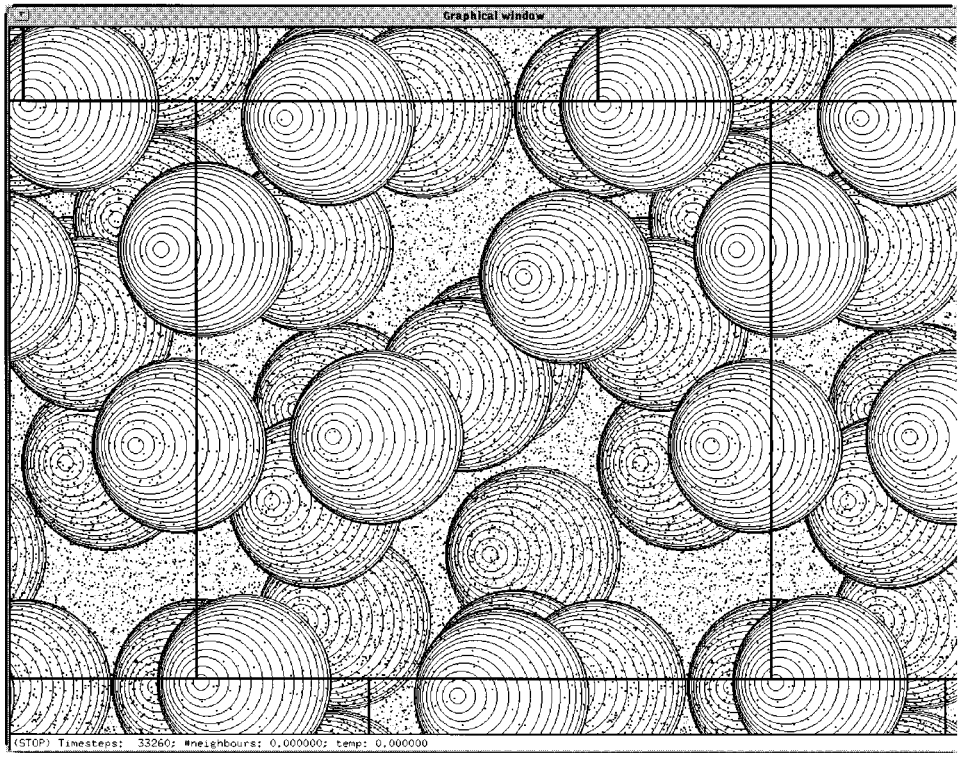

FIG. 1. Snapshot of a 30 vol % suspension of spheres. The dots are basic DPD particles, some of which are ''frozen'' into the approximately spherical particles. The steady shear is applied by sliding the periodic box above the central box to the left, and the one below to the right.

tively. The only forces acting on the spheres were the Brownian fluctuating forces and the hydrodynamic forces between the spheres, both transmitted by the fluid particles. These suspensions were subject to dimensionless steady-shear rates, varying from 3×10^{-6} to 0.05, thus covering four orders of magnitude. For each shear rate a separate simulation was performed. The shear stress was measured at each time step, and the viscosity was then calculated as an average over all the steps. Measurements of the viscosity for the higher-shear rates are obtained within a few tens of thousands of DPD steps, which take a couple of hours on a Silicon Graphics R10000 processor. In order to get acceptable statistics for the shear stress signal: noise ratio, the low-shear rates required several hundreds of thousands of time steps. This takes several days of computing time on a Silicon Graphics R10000. The solvent viscosity η_s, obtained from a simulation without suspended particles, was found to be constant at a value of 0.0362 in this shear rate regime. (Note that for $\dot{\gamma}>0.1$, the solvent as well as the sheared suspensions become unstable and the measured viscosity and kinetic energy increase dramatically.) The reduced viscosity is then calculated as the suspension viscosity divided by the solvent viscosity. Our calculated viscosities for the three sphere sizes are shown in Fig. 2 as a function of the Peclet number, using $3k_BT = 0.0033$.

We observe that the viscosity does not depend significantly on the sphere size. This is what one would expect. Furthermore, this figure shows that the viscosity follows a typical shear-thinning curve. Averaged over the various sphere sizes, we find that at low Peclet numbers ($\mathrm{Pe}<1$), $\eta(0)$ is fairly constant at a value of 4.5, corresponding with the first Newtonian plateau. Despite running the simulation for several hundreds of thousands of time steps, the error bars remain substantial at these low-shear rates. A shear-thinning regime is observed at higher shear rates ($1<\mathrm{Pe}<10$) followed by a second Newtonian plateau, where $\eta(\infty)$ is constant at a value of 3.0. The actual values for the low- and high-shear viscosities are in good agreement with the experimental results (3.77 and 2.99, respectively [1]). The characteristic viscosity $\eta(\mathrm{Pe}_c)$, as defined in Eq. (9), is found to be equal to 3.7 (taking the values for high- and low-shear viscosity of 3.0 and 4.5, respectively). This value is in good agreement with the experimental value [1] of 3.4 (±0.2).

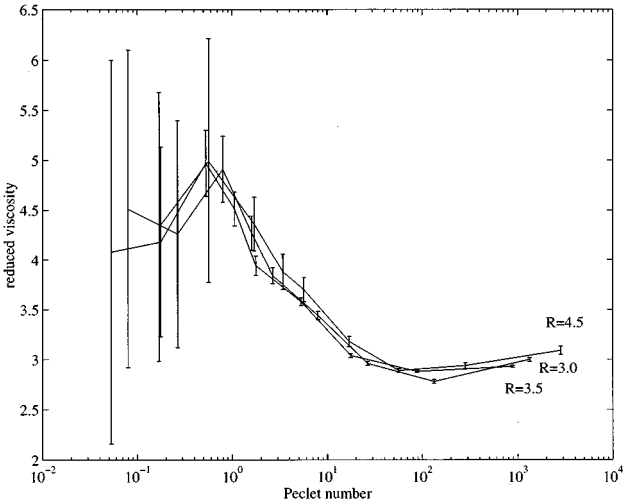

FIG. 2. Reduced viscosity of a 30% suspension of spheres as a function of Peclet number, for spheres with radii $R = 4.5$, 3.5, and 3.0.

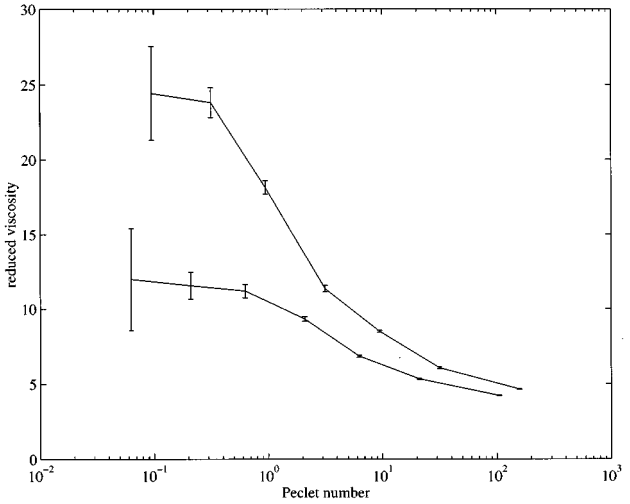

FIG. 3. Viscosity of a suspension of 40 vol % spheres as a function of Peclet number. Two different values for the radius R of the spheres has been employed: $R=3.5$ (upper curve) and $R=3.053$ (lower curve).

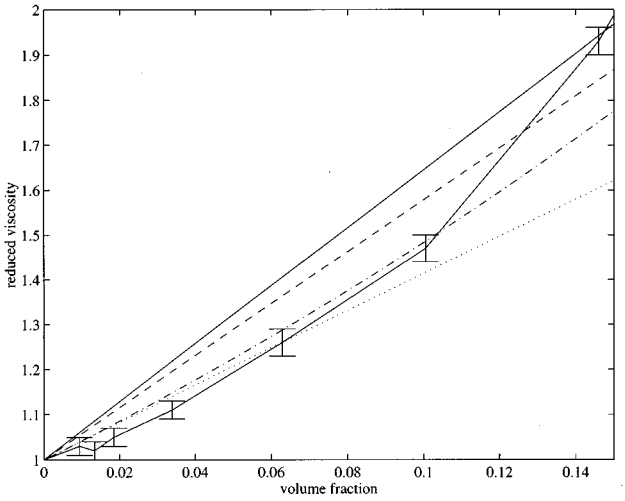

FIG. 4. Reduced viscosity of dilute suspensions of prolate ellipsoids as a function of solid volume fraction, at a steady-shear rate $\dot{\gamma}=0.0003$ (solid line with error bars, representing rms deviations). Theoretical expansions in the volume fraction are also shown for an aspect ratio $f=5$, as derived by Onsager (dotted line), Simha (dashed line), Kuhn and Kuhn (solid line), and Berry and Russel (dashed-dotted line).

Using a smaller box size of $20\times20\times20$ (containing 24 000 DPD particles), we obtain the same value for the high-shear viscosity of a 30% sphere suspension. The low-shear viscosity on the other hand is found to be significantly larger (5.5) for a sphere size of 3.053. This may be attributed to finite size effects and will be discussed in Sec. V.

We have also investigated the shear-thinning behavior of a suspension containing a higher volume fraction of spheres. Sixty-one spheres with radius 3.5 were defined within a cubic box of size $30\times30\times30$ to generate a sphere suspension of 40% by volume. Simulations were performed at shear rates in the range $3\times10^{-6}\leqslant\dot{\gamma}\leqslant5\times10^{-2}$. The measured viscosities are shown in Fig. 3 as a function of Peclet number $\mathrm{Pe}=\dot{\gamma}a^2/D_0$. With increasing shear rate, the viscosity values for the spheres with radius 3.5 (upper curve in Fig. 3) show qualitatively the correct shear-thinning behavior, exhibiting both a first and second Newtonian plateau. The value for the high-shear viscosity $\eta(\infty)$ is found to be 4.5, which compares reasonably with experimental values of 5.1 [1] and 5.9 [47]. However, the value for the low-shear viscosity $\eta(0)$ of 24.0, is much too large, as compared with the experimental values of 7.8 [1] and 10.1 [47]. Initially, we believed that this discrepancy was due to inadequate representation of intersphere lubrication: the average surface-to-surface distance is only a few times the coarse-graining length r_c. In order to check this hypothesis, we repeated the calculations for 91 spheres with a radius of 3.053, in a computational box of size $30\times30\times30$. The results of these calculations are shown in Fig. 3 as well, in the lower curve. The low-shear viscosity is much smaller now, having a value of 12.0, which is in good agreement with the aforementioned experimental data. This is somewhat surprising, because the larger the radius of the spheres, the more accurate lubrication by the surrounding DPD fluid particles should be represented (at constant volume fraction). Such behavior may be ascribed to finite size effects, which will be discussed in Sec. V.

B. Repulsive rod suspensions

To study hard rod suspensions, we have added prolate ellipsoids to the simulation, in random positions and orientations within the simulation box. The aspect ratio $f=\frac{a}{b}$ of the prolate ellipsoids was chosen to be equal to 5, with a length $2a=8$ and diameter $2b=1.6$. Up to 260 ellipsoids were defined within a simulation box of size $20\times20\times20$, to obtain volume fractions ϕ up to 35%. (MD simulations pin point the isotropic-nematic ($I\rightarrow N$) transition for hard prolate ellipsoids of $f=5$ at a volume fraction of about 37% [48]; our particles are somewhat soft, so we expect their $I\rightarrow N$ transition at densities quite higher than this.) These suspensions were subject to steady dimensionless shear rates of 3×10^{-4} and 3×10^{-5}, corresponding to Peclet numbers $\mathrm{Pe}=\dot{\gamma}a^2/D_0$ of 0.1 and 1.0, respectively. The viscosity values for dilute suspensions up to 15 vol %, at a shear rate of 3×10^{-4}, are shown in Fig. 4. In this figure, theoretical expressions for the viscosity of dilute rod suspensions are shown as well, as linear expansions in the volume fraction, according to Eq. (10). The values for the intrinsic viscosity k_1 (the slopes of these graphs), are calculated according to Eqs. (12)–(14). Given the aspect ratio $f=5$, we find intrinsic viscosity values of 4.14, 5.78, and 6.45 from the Onsager (12), Kuhn and Kuhn and Simha (13) expressions, respectively. Fitting our data by a quadratic function for $\phi<0.14$, we find a linear coefficient of 4.0, which can be interpreted as the intrinsic viscosity k_1. A quadratic coefficient of 10 is obtained, which is of the same order of magnitude as the Berry-Russel [38] prediction $(2/5)k_1^2=7$. Note that agreement cannot be expected to be quantitative, owing to the low aspect ratio of our particles (recall that the Berry-Russel prediction assumes that $f\gg1$). From 14% upward, a higher order dependence of the viscosity on the volume fraction sets in. In Fig. 5, the viscosity of these rod suspensions is shown

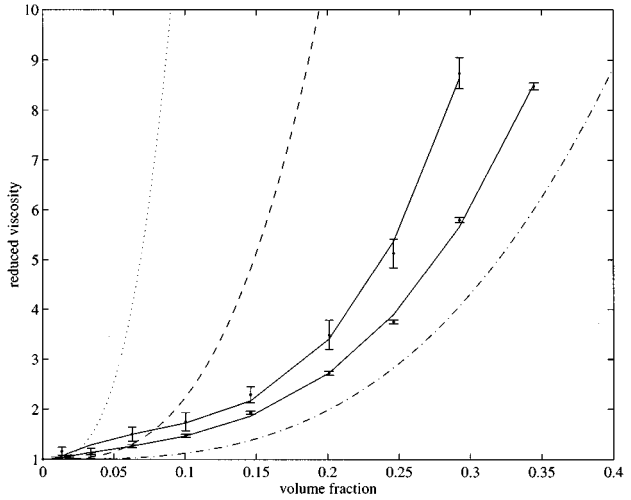

FIG. 5. Reduced viscosity of suspensions of prolate ellipsoids as a function of solid volume fraction, at steady shear rates $\dot{\gamma}$ of 0.0003 (lower curve) and 0.000 03 (higher curve). The error bars represent rms fluctuations. The polynomial fits are indicated as solid lines. As a guide to the eye equation (15) has also been drawn for $\beta=10^2$ (dotted line), 10^3 (dashed line), and 10^4 (dashed-dotted line) with α fixed at a value of zero.

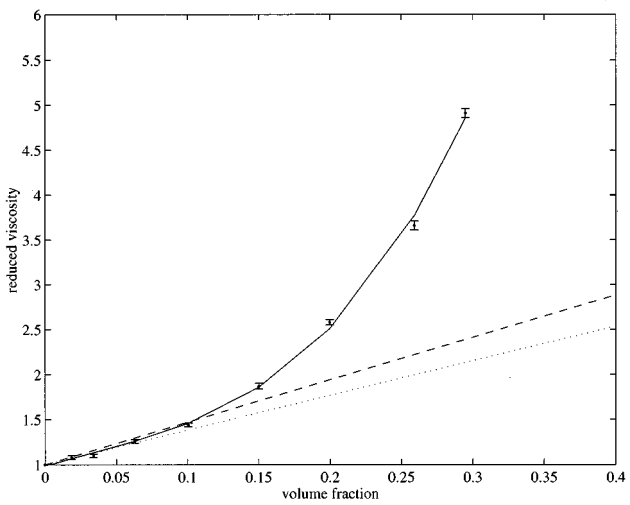

FIG. 6. Reduced viscosity of suspensions of oblate ellipsoids as a function of solid volume fraction at a steady-shear rate $\dot{\gamma}=0.0003$. Theoretical expansions in the volume fraction are shown for an aspect ratio $f=5$, as derived by Kuhn and Kuhn (dotted line) and Güven (dashed line). The polynomial fit is indicated as a solid line.

up to 35% volume fraction, for both applied shear rates. The values of the viscosity, measured at the high-shear rate, are below the ones for the lower shear rate, for each value of the volume fraction. This is what one would expect, assuming the rods orient themselves in the flow field at high-shear rates, leading to shear-thinning behavior. The higher order dependence of the viscosity on the volume fraction for $\phi>0.13$ marks the transition from the dilute regime to the concentrated regime, where the density is greater than roughly one particle per average hard-core excluded volume [49]. (For our ''soft'' rods, this value should be considered as the lower limit.) Equations (14) and (15) suggest that, in order to describe the viscosity as a function of volume fraction over the whole range of concentrations, we have to include the linear and quadratic expansions in the dilute regime as well as the third-power dependence in the concentrated regime. Therefore we have fitted our data to a third degree polynomial function. The results are presented in Fig. 5, and show a good fit to the viscosity curves for both shear rates. The cubic term coefficients for the high- and low-shear rates are 222 and 584, respectively. It may be possible to relate these coefficients to the β factor in Eq. (15) although this should be treated with care because we neglect log jamming effects by effectively setting $\alpha=0$. As a guide to the eye, we have plotted Eq. (15) for several values of the β parameter in Fig. 5. Our curves correlate with $10^3<\beta<10^4$, which is roughly in agreement with the experimental value of $\beta=8600$ for a solution of xanthan gum [38]. Summarizing, we can say that our results are in agreement with the Doi-Edwards third-power scaling law. The expression ''scaling law'' is justified in this context, because the viscosity contributions of the first and second order terms in ϕ are relatively small compared to the third order contribution.

We have also performed simulations of prolate ellipsoids with a larger aspect ratio of 10. Because the array dimensions of the Rheoflex code limit the number of DPD particles and therefore the simulation box dimensions at a constant density of 3, we had to use thin ellipsoids with a diameter $2b=0.8$. We found that the viscosity of such suspensions did not show the expected increase as a function of solid volume fraction. The reason for this is probably that the ellipsoids have effectively become too thin. The hydrodynamic interaction radius r_c of the DPD particles was chosen to be equal to one. Therefore the solvent particles on opposite sides of the long dimension of the ellipsoids will be able to interact, as they are separated by a distance $2b=0.8$. Hence, the rod particles may become effectively ''transparent'' for the solvent, which causes the unexpectedly low viscosity. For this reason it is important to select the dimensions of solid objects carefully.

C. Repulsive disk suspensions

In order to model suspensions of disks, we have added oblate ellipsoids to the simulation, having an initially random position and orientation. The aspect ratio of the disks was chosen to be equal to 1/5, whereas the volume of the disk was equal to the one of the aforementioned prolate ellipsoid. Up to 225 ellipsoids were defined within a simulation box of size $20\times20\times20$, to obtain volume fractions up to 30%. These suspensions were simulated at a steady-shear rate of 3×10^{-4}. The reduced viscosity of the oblate ellipsoid suspensions is shown in Fig. 6. As in the case of our simulations of the rod suspensions, we have fitted our viscosity values to a third degree polynomial function. The result is presented in Fig. 6, and our data show a good fit to the cubic function. Note that suspensions of spheres also show this third order behavior up to $\phi\simeq0.35$ [50]. This agreement may be explained by the fact that, thermodynamically, disks behave very much like spheres (the excluded volume of a sphere is approximately equal to that of a disk), and therefore disks

may conform to a similar ''virial'' expansion. Returning to our viscosity data, we find a linear coefficient of 4.71, which can again be interpreted as the intrinsic viscosity. This result is in excellent agreement with the value of 4.71 as derived from the expression by Güven [Eq. (17)], and compares reasonably to the Kuhn and Kuhn prediction of 3.84 [Eq. (16)]. The third degree coefficient has a value of 147, which is lower than for rod suspensions (222 at the same shear rate). One might speculate that the number of solid objects needed for jamming or entanglement is lower for rods than for disks.

Note that, even in the case of an aspect ratio as low as $f=5$, the intrinsic viscosity of rodlike particles ($k_1 = 5.67$ in our case) is higher than the intrinsic viscosity of a suspension of disks having the same aspect ratio. This is in general agreement with previous observations [46]. Summarizing, we confirm the theoretical linear behavior at low volume fractions and predict a third-power scaling law for concentrated suspensions of disks.

V. DISCUSSION OF FINITE SIZE AND RESOLUTION EFFECTS

In this section we want to discuss the finite size effects observed in our simulations of sphere suspensions, and clarify the difference between ''finite size effects'' and ''resolution effects.'' The latter may be attributed to the fact that the solvent particles are not of negligible size compared to the colloidal particulates, and, hence, the continuum limit is not obeyed.

For a 30% sphere suspension in a $30\times30\times30$ system size, we observed that spheres of sizes 3, 3.5, and 4.5 give essentially the same results for the viscosity. This implies two independent things: (1) The size of the system (in terms of number of colloidal particles) is large enough. (2) A resolution as small as 3:1 is also enough. Here 3 refers to the radius of the sphere and 1 to the radius of the fluid particles. The ''continuum limit'' seems to be achieved already because by increasing the resolution to 4.5:1 nothing is gained. Using larger particles it may be expected that finite size effects will show up.

For a 30% sphere suspension in a $20\times20\times20$ system, we observed that the low-shear viscosity is too large. It may be expected that the results will get worse as the radius increases. In order to investigate this point, we have performed simulations for different sphere sizes at a constant 30% volume fraction. Indeed, we found that the low-shear viscosity increases systematically from 5.5 to 6.6 with sphere sizes increasing stepwise from 3.0 to 4.5. This implies that the continuum limit is well represented, as the resolution 3:1 is sufficient, but the system size is actually too small.

At 40% volume fraction, we observed that, for a $30\times30\times30$ system size, spheres of sizes 3 and 3.5 give different results for the viscosity; the result for the small spheres is better. In this simulation the resolution 3:1 seems to be fine but what fails is the system size. Increasing the resolution to 3.5:1 yields no improvement because the system size is then too small. For this reason it may be expected that, considering a sphere size of 3 (resolution 3:1) in a smaller system ($20\times20\times20$), the results will worsen in the same direction as by increasing the radius to 3.5 in the bigger system ($30\times30\times30$). Indeed, from simulations performed for both systems mentioned, we observed that the low-shear viscosities are 28.7 and 24.0, respectively, compared to a value of 12.0 for the spheres of size 3.0 in the bigger system.

One may speculate that the reason why finite size effects arise sooner for concentrated suspensions can be attributed to direct interactions between colloidal particles. In principle, two colloidal particles that are in contact can interpenetrate because they are ''soft.'' Note that at high concentrations interpenetration is more favorable, due to lack of available free volume. A suspension of interpenetrating spheres may have enhanced viscosity because of the fact that the particles are rigid bodies. In a sense, if the particles are rigid and they are ''anchored'' to each other (through interpenetration) the overall response of the system could be more ''rigid,'' that is more viscous. In other words, if the colloidal particles are forced into one another's interaction radius, the dissipative term in Eq. (3) will increase. This could lead to an increase of viscosity for the large spheres over that for the small spheres just as we have found. This effect manifests itself mainly at low-shear rates; at high-shear rates, the structure present in the suspension is suppressed by the applied shear, and the situation is in a sense similar to a dilute suspension.

In summary, it seems that in all the cases considered the resolution is sufficient (even in the 40% suspension). However, there are finite size effects that are more important as the volume fraction increases.

VI. CONCLUSIONS

We have performed simulations of the rheology of dense particulate suspensions using a mesoscopic simulation technique, known as dissipative particle dynamics. Within the flexible environment of the Rheoflex DPD code, it is easy to define solid particulates of various sizes and shapes. In this report we have studied the steady-shear flow of suspensions of spheres, rods, and disks at various concentrations and shear rates. For sphere suspensions up to 30%, we find shear-thinning behavior consistent with experiment; the values of both the high- and low-shear viscosity are, in fact, in good agreement with experimental results. Furthermore, these results are independent of the size of the suspended spheres. Denser suspensions (40%) give good results for the high-shear viscosity; for low-shear rates, however, the size of the simulation box should be augmented to eliminate finite size effects. Therefore, we consider DPD to be a valuable alternative to Brownian and Stokesian dynamics as a simulation method for studying particulate suspensions, particularly at higher-shear rates; as with other methods, at lower-shear rates, in the regime where Brownian motion dominates, the computing time required to obtain statistically significant results increases strongly.

Dilute suspensions of rods and disks, subject to a steady-shear rate, show a linear increase in the reduced viscosity with increasing volume fraction. The slopes of these functions, corresponding to the intrinsic viscosities of rods and disks, respectively, are in excellent agreement with theoretical linear expansions as a function of the aspect ratio. At higher concentrations, in the concentrated regime, our viscosity data for both rods and disks scale with the third power of the volume fraction. For suspensions of rods, this scaling behavior is consistent with a theoretical expression derived by Doi and Edwards [39] for the semidilute regime.

In conclusion, we have shown that the DPD simulation technique produces realistic hydrodynamic behavior for complex suspensions containing solid objects of various sizes and shapes. Therefore, we believe that DPD is a powerful tool for studying the flow behavior of complex colloidal fluids.

ACKNOWLEDGMENTS

We are grateful to Antoine Schlijper and Shell Research for making the Rheoflex DPD code available, and to Pep Español, David Heyes, and John Melrose for stimulating discussions.

[1] J. van der Werff and C. de Kruif, J. Rheol. **33**, 421 (1989).
[2] D.M.E. Thies-Weesie, A.P. Philipse, and H.N.W. Lekkerkerker, J. Colloid Interface Sci. **177**, 427 (1996).
[3] C. Chang and R.L. Powell, J. Fluid Mech. **253**, 1 (1993).
[4] N.J. Wagner and A.T.J.M. Woutersen, J. Fluid Mech. **278**, 267 (1994).
[5] W.B. Russel, J. Rheol. **24**, 287 (1980).
[6] A.M. Wierenga and A.P. Philipse, J. Colloid Interface Sci. **180**, 360 (1996).
[7] P.J. Mitchell, D.M. Heyes, and J.R. Melrose, J. Chem. Soc. Faraday Trans. **91**, 1975 (1995).
[8] T.N. Phung, J.F. Brady, and G. Bossis, J. Fluid Mech. **313**, 181 (1996).
[9] A.J.C. Ladd, Phys. Rev. Lett. **70**, 1339 (1993); A.J.C. Ladd, J. Fluid Mech. **274**, 285 (1994); **274**, 311 (1994); A.J.C. Ladd, Hu Gang, J.X. Zhu, and D.A. Weitz, Phys. Rev. Lett. **74**, 318 (1995).
[10] P.N. Segrè, O.P. Behrend, and P.N. Pusey, Phys. Rev. E **52**, 5070 (1995).
[11] C.P. Lowe and D. Frenkel, Phys. Rev. E **54**, 2704 (1996).
[12] P.J. Hoogerbrugge and J.M.V.A. Koelman, Europhys. Lett. **19**, 155 (1992).
[13] G.K. Batchelor, in *Theoretical and Applied Mechanics*, edited by W.T. Koiter (North-Holland, Amsterdam, 1976), pp. 33–55.
[14] J.M.V.A. Koelman and P.J. Hoogerbrugge, Europhys. Lett. **21**, 369 (1993).
[15] A.G. Schlijper, P.J. Hoogerbrugge, and C.W. Manke, J. Rheol. **39**, 567 (1995).
[16] Y. Kong, C.W. Manke, W.G. Madden, and A.G. Schlijper, Int. J. Thermophys. **15**, 1093 (1994).
[17] P.V. Coveney and K.E. Novik, Phys. Rev. E **54**, 5134 (1996).
[18] P. Español, Phys. Rev. E **52**, 1734 (1995).
[19] P. V. Coveney and P. Español, J. Phys. A **30**, 779 (1997).
[20] P. Español and P. Warren, Europhys. Lett. **30**, 191 (1995).
[21] P.J. Hoogerbrugge, RHEOFLEX User Guide, KSEPL, 1992.
[22] A.W. Lees and S.F. Edwards, J. Phys. C **5**, 1921 (1972).
[23] I.M. Krieger, Adv. Coll. Int. Sci. **3**, 111 (1972).
[24] The colloid density ρ should not be confused with the DPD fluid density n, as defined in Sec. II.
[25] A. Einstein, Ann. Phys. (N.Y.) **19**, 289 (1906); **34**, 591 (1911).
[26] G.K. Batchelor and J.T. Green, J. Fluid Mech. **56**, 401 (1972).
[27] G.K. Batchelor, J. Fluid Mech. **83**, 97 (1977).
[28] I.M. Krieger and T.J. Dougherty, Trans. Soc. Rheol. **3**, 2817 (1959).
[29] R. Ball and P. Richmond, J. Phys. Chem. Liq. **9**, 99 (1980).
[30] D. Quemada, Rheol. Acta **16**, 82 (1977).
[31] H.A. Barnes, M.F. Edwards, and L.V. Woodcock, Chem. Eng. Sci. **42**, 591 (1987).
[32] B.I.M. ten Bosch and P.J. Hoogerbrugge, *Proccedings of the Fourth European Rheology Conference, Sevilla, 1994*, edited by C. Gallegos, A. Guerrero, J. Munoz, and M. Berjano (Steinkopff, Darmstadt, 1994), p. 687.
[33] We define the volume fraction colloidal spheres in our simulations as $\phi=(4/3)\pi a^3 N/L^3$, where a is the radius and N is the total number of colloidal particles, and L is the length of the cubic simulation box.
[34] L. Onsager, Phys. Rev. **40**, 1028 (1932).
[35] R. Simha, J. Phys. Chem. **44**, 25 (1940).
[36] W. Kuhn and H. Kuhn, Helv. Chim. Acta **28**, 97 (1945).
[37] J.M. Burgers, Verh. Akad. Amsterdam **16**, 113 (1938), [4].
[38] D.H. Berry and W.B. Russel, J. Fluid Mech. **180**, 475 (1987).
[39] M. Doi and S.F. Edwards, *The Theory of Polymer Dynamics* (Oxford University Press, New York, 1986).
[40] M. Doi, J. Phys. (France) **36**, 607 (1975).
[41] T. Sato and A. Teramoto, Macromolecules **24**, 193 (1991).
[42] I. Bitsanis, H.T. Davis, and M. Tirrell, Macromolecules **21**, 2824 (1988).
[43] I. Bitsanis, H.T. Davis, and M. Tirrell, Macromolecules **23**, 1157 (1990).
[44] Y. Takada, T. Sato, and A. Teramoto, Macromolecules **24**, 6215 (1991).
[45] L. Onsager, Ann. N.Y. Acad. Sci. **51**, 627 (1949).
[46] N. Güven, *Clay-Water Interface and its Rheological Implications* (The Clay Minerals Society Boulder, CO, 1992); Chap. 2.
[47] P.N. Segrè, S.P. Meeker, P.N. Pusey, and W.C.K. Poon, Phys. Rev. Lett. **75**, 958 (1995).
[48] G.J. Vroege and H.N.W. Lekkerkerker, Rep. Prog. Phys. **55**, 1241 (1992); M.P. Allen and M.R. Wilson, J. Comp. Aided Mol. Design **3**, 335 (1989).
[49] B. Tjipto-Margo and G.T. Evans, J. Chem. Phys. **93**, 4254 (1990).
[50] C.G. de Kruif, E.M.F. van Iersel, A. Vrij, and W.B. Russel, J. Chem. Phys. **83**, 4717 (1985); D. Bedeaux, J. Colloid Interface Sci. **118**, 80 (1987).